Journal Pre-proofs

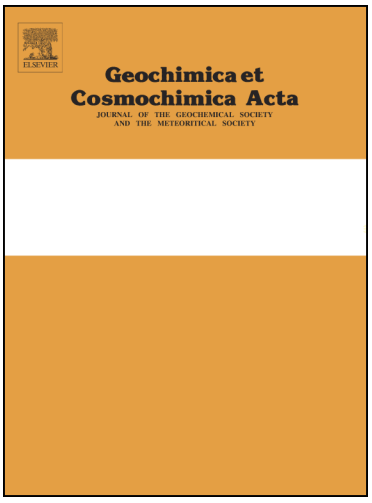

Sr in coccoliths of *Scyphosphaera apsteinii*: partitioning behavior and role in coccolith morphogenesis

Erin M. Meyer, Gerald Langer, Colin Brownlee, Glen L. Wheeler, Alison R. Taylor

PII: S0016-7037(20)30400-2
DOI: https://doi.org/10.1016/j.gca.2020.06.023
Reference: GCA 11815

To appear in: *Geochimica et Cosmochimica Acta*

Received Date: 19 February 2020
Revised Date: 29 May 2020
Accepted Date: 23 June 2020

Please cite this article as: Meyer, E.M., Langer, G., Brownlee, C., Wheeler, G.L., Taylor, A.R., Sr in coccoliths of *Scyphosphaera apsteinii*: partitioning behavior and role in coccolith morphogenesis, *Geochimica et Cosmochimica Acta* (2020), doi: https://doi.org/10.1016/j.gca.2020.06.023

Sr in coccoliths of *Scyphosphaera apsteinii*: partitioning behavior and role in coccolith morphogenesis

Erin M. Meyer[a], Gerald Langer[b], Colin Brownlee[b,c], Glen L. Wheeler[b] & Alison R. Taylor[a]

[a]Department of Biology and Marine Biology, University of North Carolina Wilmington, Wilmington, NC, 28403, USA.

[b]Marine Biological Association, The Laboratory, Citadel Hill, Plymouth, Devon PL1 2PB, UK.

[c]School of Ocean and Earth Science, University of Southampton, Southampton, SO14 3ZH, UK.

Correspondence:

Alison R. Taylor – taylora@uncw.edu, corresponding author.

Erin M. Meyer – emm5468@uncw.edu

Gerald Langer – gerlan@mba.ac.uk

Colin Brownlee – cbr@mba.ac.uk

Glen L. Wheeler – glw@mba.ac.uk

Abstract

Coccolithophores are important contributors to global calcium carbonate through their species-specific production of calcite coccoliths. Nannofossil coccolith calcite remains an important tool for paleoreconstructions through geochemical analysis of isotopic and trace element incorporation including Sr, which is a potential indicator of past surface ocean temperature and productivity. *Scyphosphaera apsteinii* (Zygodiscales) exhibits an unusually high Sr/Ca ratio and correspondingly high partitioning coefficient (D_{Sr} = 2.5) in their two morphologically distinct types of coccoliths: flat muroliths and barrel-like lopadoliths. Whether or not this reflects mechanistic differences in calcification compared to other coccolithophores is unknown. We therefore examined the possible role of Sr in *S. apsteinii* calcification by growing cells in deplete (0.33 mmol/mol Sr/Ca), ambient (9 mmol/mol Sr/Ca), and higher than ambient Sr conditions (36 and 72 mmol/mol Sr/Ca). The effects on growth, quantum efficiency of photosystem II (F_v/F_m), coccolith morphology, and calcite D_{Sr} were evaluated. No effect on *S. apsteinii* growth rate or F_v/F_m was observed when cells were grown in Sr/Ca between 0.33 - 36 mmol/mol. However, at 72 mmol/mol Sr/Ca growth rate was significantly reduced, although F_v/F_m was unaffected. Reducing the Sr/Ca from ambient (9 mmol/mol) did not significantly alter the frequency of malformed and aberrant muroliths and lopadoliths, but at higher than ambient Sr/Ca conditions coccolith morphology was significantly disrupted. This implies that Sr is not a critical determining factor in normal coccolith calcite morphology in this dimorphic species. Using energy dispersive spectroscopy (EDS) we observed an increase in [Sr] and decrease in D_{Sr} of coccoliths as the Sr/Ca of the growth medium increased. Interestingly, muroliths had significantly lower Sr/Ca than lopadoliths at ambient and elevated [Sr], and lopadolith tips had lower Sr than bases in ambient conditions. In summary, the Sr fractionation behavior of *S. apsteinii* is distinct from other coccolithophores because of an unusually high D_{Sr} and inter- and

intra-coccolith variability in Sr/Ca. These observations could be explained by mechanistic differences in the selectivity of the Ca^{2+} transport pathway or in the Sr-and Ca-binding capacity of organic components, such as polysaccharides associated with coccolithogenesis.

1.0 Introduction

Coccolithophores are unicellular marine algae that produce $CaCO_3$ plates (coccoliths) intracellularly that are secreted onto the cell surface where they collectively form the calcite coccosphere (Young et al., 1999). Coccolithophores contribute roughly half of global $CaCO_3$ production, producing ~ 1 – 1.42 Gt C yr^{-1} (Daniels et al., 2018; Hopkins and Balch, 2018; Milliman, 1993). Therefore, coccolithophores have a significant impact on ocean biogeochemical cycles through calcification, photosynthesis, and ultimately carbon export (Balch, 2018; Krumhardt et al., 2017; Taylor et al., 2017). Nannofossil coccolith calcite is widely used in micropaleontology, biostratigraphy, and for paleo-reconstructions of ocean ecosystem dynamics (Flores et al., 1997; Saavedra-Pellitero et al., 2017; Stoll et al., 2007a; Stoll et al., 2007b; Young et al., 2014). This is partly due to their distinct morphologies, but also because stable isotope and cation fractionation in coccolith calcite provides tools that can aid paleoreconstructions of oceanic conditions at the time of precipitation.

Past studies have found detectable amounts of strontium (Sr) in coccoliths (Hermoso et al., 2017; Rickaby et al., 2002; Stoll et al., 2002b), and $^{88/86}Sr$ isotope ratios (seawater:calcite) have been used to model past seawater temperature, Sr cycling, and carbonate chemistry (Müller et al., 2018). Calcite Sr/Ca ratios have also been examined in relation to coccolithophore growth and calcification rates as a measure of ocean productivity. Stoll et al. (2007b) used coccoliths from sediment traps to determine species-specific Sr/Ca ratios, which could then be used to estimate seasonal fluxes of $CaCO_3$ export. Rickaby et al. (2002) found a positive relationship between growth rate and the Sr incorporation for *Emiliania huxleyi* grown under nitrogen limitation. Sr incorporation into coccoliths also increased with increased rates of calcification

and carbon fixation (Rickaby et al., 2002). However, light induced changes in growth and calcification rate did not affect Sr partitioning (Langer et al., 2006; Stoll et al., 2002a; Stoll et al., 2002b). Therefore, growth and calcification rate per se do not influence Sr partitioning, but some physiological processes altered by nitrogen limitation do (Langer et al., 2006). Through understanding the relationship between Sr incorporation and carbon-specific growth rate, Rickaby et al. (2002) suggested Sr/Ca ratios and ε_p (the difference in $\delta^{13}C$ between dissolved inorganic carbon and organic matter) in coccolithophores could be used as a potential proxy for past surface pCO_2 levels. Variations in cation incorporation can also suggest evolutionary links between extinct and extant coccolithophore species. Based on lower Sr/Ca ratios, Sucheras-Marx et al. (2016) inferred that the mid-Jurassic *Watznaueria britannica* might have been adapted for oligotrophic waters, with slower growth rates than modern equivalent species.

Coccolithophores require one of the highest Ca^{2+} fluxes across the plasma membrane in order to sustain calcification (Brownlee and Taylor, 2004; Brownlee et al., 2015; Taylor et al., 2017), and have multiple modes of Ca^{2+} selective transport both into the cell and to various organelles and compartments (Hermoso, 2014; Mackinder et al., 2010; Marsh, 2003; Outka and Williams, 1971). Because Sr^{2+} has a similar electron configuration and chemical properties to Ca^{2+}, it can potentially enter the cell through Ca^{2+} transporter proteins or channels with a relatively high Sr permeability. This is supported by Sr and Ca isotope fractionation that suggests they share the same transport pathway (Müller et al., 2018; Stevenson et al., 2014). Indeed, Sr^{2+} has been used as a Ca^{2+} analogue to trace the Ca^{2+} transport pathway in *E. huxleyi* (Gal et al., 2017). Multiple studies have calculated partitioning coefficients (D_{Sr}) from coccolith Sr/Ca ratios resulting in D_{Sr} values varying between 0.02 – 0.6 for various coccolithophore species including *E. huxleyi, Gephyrocapsa oceanica,* and *Coccolithus braarudii* (Table 1). *Scyphosphaera*

apsteinii is notable for its massive barrel-like lopadoliths and ovoid muroliths (Fig. 1A-B; Drescher et al., 2012); that have an unusually high Sr/Ca ratio of 22.1 mmol/mol and D_{Sr} of 2.5 (Hermoso et al., 2017) which is an order of magnitude greater than other extant species, implying mechanistic differences in calcite production in *S.apsteinii* that leads to increased Sr/Ca at the site of calcification and in the coccolith. In order to better understand the atypical Sr fractionation behavior in *S. apsteinii*, we designed experiments to explore the requirement for Sr and its incorporation in muroliths and lopadoliths. We hypothesized that the high Sr/Ca of *S. apsteinii* coccoliths is required for normal morphogenesis, either directly in the calcite lattice or indirectly through an association with organic components. To test this hypothesis, we grew *S. apsteinii* in an artificial seawater medium (Aquil media) containing a range of Sr concentrations (3.3 -720 μM; normal seawater has ~ 90 μM Sr, De Villiers, 1999), and used analytical scanning electron microscopy (SEM) combined with energy dispersive spectroscopy (EDS) to analyze coccolith morphology and Sr/Ca ratios. We show that high levels of Sr incorporation into *S. apsteinii* coccoliths observed under ambient Sr/Ca is not required for normal morphology, however higher than ambient Sr/Ca gave rise to an increased frequency of malformations.

2.0 Methods

2.1 Maintenance of algal cultures, experimental media, and growth conditions

S. apsteinii strain RCC 1456 was obtained from the Roscoff Culture Collection, France and maintained according to Drescher et al. (2012). Experimental cultures were grown in 40 mL polystyrene flasks in an artificial seawater, Aquil media, modified from (Kester et al., 1967) by adding f/8 metals, f/8 vitamins, 1 mL/L of sterilized Gulf Stream seawater, and modifying the following nutrients: 64 μM NO_2^-, 4 μM PO_4^3, and 10 nM SeO_2. The [Ca] was 10 mM, and the

[Sr] of the Aquil medium was 3.3 μM as determined using ICP-MS. Media pH was measured, ranging from 7.93 – 7.96 and the [HCO_3^-] was 2.3 mM. A 1M $SrCl_2 \cdot 6H_2O$ stock solution (Puratronic, 99.9965%, 10877, Alfa Aesar) was used to amend the [Sr] of the Aquil media from 3.3 (no added Sr), to 90, 360, and 720 μM Sr (giving rise to 0.33, 9, 36 and 72 mmol/mol Sr/Ca respectively). Because stock cultures of *S. apsteinii* are grown in a natural seawater media with a [Sr] of 95.4 μM (verified using ICP-MS), the cells were acclimated for at least 8 generations in the corresponding Aquil/Sr medium to ensure all attached coccoliths were produced in the presence of the treatment [Sr]. All cultures were maintained at 15°C on a 14:10 h light:dark cycle, at approximately 100 μmol m^{-2} s^{-1} with sub-culturing at mid-late exponential growth phase.

Cultures acclimated to each [Sr] treatment were harvested at mid-exponential growth (~$1x10^4$ cells mL^{-1}) and used to establish four replicate experimental flasks with a starting density of ~$1x10^3$ cells mL^{-1}. Cell counts were recorded over 10 d using a Sedgewick-Rafter chamber with a minimum of 300 cells counted per sample. Cell densities were plotted versus time and growth rate (μ) was calculated from exponential regression including all data-points till harvest day (day 10).

The quantum yield of photosystem II (F_v/F_m) was estimated using an AquaPen AP 100 fluorometer (PSI, Drasov, Czech Republic). Approximately 1.5 mL of sample from each flask was placed in a cuvette and dark-adapted at room temperature for 15 min prior to measurements. An average of 3 measurements was taken over 3 min with cuvettes gently inverted to resuspend cells 10 s prior to each measurement.

2.2 SEM and EDS

Mid-exponential *S. apsteinii* cells were used for SEM and EDS analysis. A 1.5 mL aliquot of each replicate culture for each [Sr] treatment was syringe filtered onto 13 mm diameter, 0.4 µm pore-size Isopore filters [Merck Millipore Ltd.] followed by buffered Nanopure water (1 mM HEPES, pH 8.0) to remove salts. Filters were air-dried and mounted onto an aluminum stub with carbon adhesive tabs before coating with 10 nm Pt/Pd. Samples were analyzed using a FEI Verios 460L SEM equipped with an Oxford Xmax silicon drift EDS detector and AZtec acquisition and analysis software (Oxford Instruments, UK). The primary beam acceleration was 10 kV (EDS and electron backscatter imaging mode) or 2 kV (secondary electron imaging). For EDS, spectra were from 1-2 µm diameter regions of interest collecting for 60 s between 2,000 – 8,000 cps with an average deadtime < 5%. Peaks for major elements of coccoliths were auto-detected and Pt/Pd peaks were eliminated. Standardless quantification was used to estimate atomic % (At%) and weight % (Wt%) compositions of calcite. A power analysis suggested a minimum sample size of 12 region of interest (ROI) spectra per sample across all treatments was needed to statistically detect an effect size of ≥ 0.15 At% Sr. Ultimately, at least 31 spectra were taken for muroliths and at the base and tip of each lopadolith (Fig. 1C-D). Wt% values were used to determine Sr/Ca mmol/mol of calcite (Hermoso et al., 2017) which were subsequently used to calculate D_{Sr} (Eq. 2).

$$\text{Eq 1: } \frac{Sr\ mmol}{Ca\ mol} = 1000 * \frac{Sr\ [Wt\%]}{Ca\ [Wt\%]} * \frac{Ca\ MW}{Sr\ MW}$$

$$\text{Eq 2: } D_{Sr} = \frac{Sr/Ca\ mineral}{Sr/Ca\ medium}$$

Effects of [Sr] on coccolith morphology were determined by scoring coccoliths from 40 cells for each treatment. Coccoliths were only scored if the majority of the coccolith could be seen. Muroliths were scored into four categories: normal, malformed, incomplete, and aberrant

(see Fig. 3). Lopadoliths were scored into five categories: normal, malformed (minor malformations commonly seen in control cultures), Type S (incomplete, normal calcite morphology), Type R (longitudinal cleavage in lopadoliths), and Type T (aberrant, completely disorganized calcite; see Fig. 3). Scores for each morphometric category are presented as the average of the experimental replicates (n=4).

2.3 Statistics

A one-way ANOVA was completed in SigmaPlot 14.0 to compare differences in morphology between Sr treatments. The data was found to be not normal through a Shapiro-Wilks test, therefore we used a Tukey's pairwise comparison. A t-test was used for comparing growth rates, photosynthetic physiology, Sr/Ca mmol/mol, D_{sr}, and differences in Sr content between muroliths and lopadoliths. The data was found to be not normal through a Shapiro-Wilks test, therefore we used a Mann-Whitney Rank Sum test. Differences between Sr content in lopadolith bases and tips were analyzed using a Student's t-test.

3.0 Results

3.1 Sr effects on physiology and coccolith morphology

We grew *S. apsteinii* in deplete, ambient, and high [Sr] to assess the effects of Sr on cell physiology and coccolith morphology. There was no significant effect of low Sr on growth rate and photosynthetic physiology (Fig. 2A-B); however, cells grown in 72 mmol/mol Sr/Ca had significantly lower growth rates ($p < 0.01$; Fig. 2A). In preliminary experiments, cells were also grown in 144 mmol/mol Sr/Ca but they stopped dividing almost immediately, implying a potential Sr toxicity, and were not further analyzed. Elevated Sr is known to increase apoptosis and decrease cell division in human stem cells and maize root cells respectively, thereby

inhibiting cell growth resulting in Sr toxicity (Aimaiti et al., 2017; Kozhevnikova et al., 2009). Average F_v/F_m values ranged from 0.55 – 0.58 and were unaffected by [Sr] over the range 0.33-72 mmol/mol Sr/Ca, indicating there was no overall change of photosynthetic efficiency in either lower or higher than ambient Sr (Fig. 2B). The average coccosphere Sr/Ca, calculated by combining the calcite Sr/Ca values of both types of *S. apsteinii* coccoliths, was three times that of the ambient medium (27.0 ± 10.8 vs 9 mmol/mol; Fig. 2C-D). Coccolith calcite Sr/Ca significantly increased with increasing media [Sr] ($p < 0.001$; Fig. 2C-D; Table 2) although the corresponding D_{Sr} decreased with the relationship best described as a second-order polynomial curve ($r^2 = 0.92$; $p < 0.001$; Table 2).

Coccolithogenesis was disrupted when *S. apsteinii* were grown in higher than ambient [Sr], resulting in increased frequency of malformed and aberrant coccoliths (Fig. 3). The 0.33 mmol/mol group had the highest frequency of normal coccoliths ($p < 0.001$) and fewest morphological disruptions to their coccoliths (Fig. 3; Fig. 4), while the 72 mmol/mol group had significantly more Type R ($p < 0.001$) and Type T ($p < 0.05$) lopadolith malformations and aberrant muroliths ($p < 0.001$; Fig. 4; Table 3). Type R coccoliths were seen frequently in response to elevated Sr concentrations, showing jagged edges along the lopadolith tips (Fig. 3; Fig. 4).

3.2 Sr/Ca and D_{Sr} correlates with Sr/Ca of medium and varies between and within coccolith types

When comparing cells grown at ambient [Sr], we observed muroliths had significantly less Sr than lopadoliths (22.9 ± 10.6 and 31.1 ± 9.5 Sr/Ca mmol/mol respectively; $p < 0.001$; Fig. 5). The lower murolith Sr content was consistent among all [Sr] treatments analyzed (Fig. 5; Table 3). Correspondingly, D_{Sr} for muroliths was significantly lower than lopadoliths across all

[Sr] treatments ($p < 0.001$; Table 3). The limit of detection (LOD) for Sr using EDS was determined to be 0.2 Wt% (2.29 mmol/mol). The Sr/Ca values for coccoliths grown in the 0.33 mmol/mol Sr/Ca treatment were clearly much lower than the other treatments, but considered to be below the technical LOD and not reported here, although the technical LOD is indicated in relevant graphs.

Because of the large size of *S. apsteinii* coccoliths, the spatial distribution of Sr in lopadoliths was examined by acquiring EDS estimates of Sr/Ca from base and tip regions of these barrel-like structures (Fig. 1C-D). Lopadolith tips had a small but significantly lower Sr incorporation compared to bases in cells grown in ambient [Sr] (28.8 ± 9.87 and 33.6 ± 8.51 Sr/Ca mmol/mol respectively; $p < 0.05$; Fig. 5), although the calculated D_{Sr} values were lower but not significant ($p = 0.05$) between tip and base. The spatial difference in Sr/Ca between base and tip was not significantly different in cells grown at higher than ambient [Sr] (Fig. 5; Table 3).

4.0 Discussion

4.1 Fractionation for Sr in S. apsteinii

Our results are consistent with Hermoso et al. (2017) in that there is unusually high Sr/Ca in *S. apsteinii* calcite compared to other species. We also observed an increase in coccolith Sr/Ca and a decrease in D_{Sr} with increasing media Sr concentrations, which is in line with several studies on a variety of species (Table 1) (Hermoso et al., 2017; Payne et al., 2008; Sun et al., 2018). Coccolithophores exhibit a range of Sr/Ca ratios (Prentice et al., 2014; Stoll et al., 2002b; Stoll et al., 2007b) with a trend for small coccolithophores such as *E. huxleyi* and *G. oceanica* significantly fractionating against Sr, yielding Sr/Ca ratios of ~3 and 1.2 mmol/mol respectively

(Hermoso et al., 2017; Stoll et al., 2002a). This relationship appears to also hold true for mixed field samples in which sediments with an abundance of larger species bearing bulky coccoliths such as *Calcidiscus leptoporus* are associated with higher Sr/Ca ratios (between 2 and 2.4 mmol/mol) than sediments dominated by smaller species such as *E.huxleyi* (Stoll and Schrag, 2000). The D_{Sr} in *S. apsteinii* at ambient [Sr] (D_{Sr} = 3, this study) is similarly much higher when compared to other species (Table 1).

To explain the unusually high Sr/Ca ratio in *S.apsteinii,* Hermoso et al. (2017) proposed a multi-step cellular process whereby Ca^{2+} channels in the plasma membrane fractionate in favor of Sr with additional fractionation for Sr through intracellular Ca^{2+} transport through an unexplained mechanism. A Ca^{2+} return flux from the CV into the cytosol through Ca^{2+} channels is also proposed to fractionate against Sr, further enriching Sr at the site of mineralization. We offer several additional perspectives to interpret the high Sr content observed in *S. apsteinii* coccoliths.

Fractionation by plasmamembrane Ca^{2+} channels for Sr^{2+} as proposed by Hermoso et al. (2017) could explain the high D_{Sr} of *S. apsteinii*. In fact, a higher Sr^{2+} permeability ($Sr^{2+} > Ca^{2+}$) has been demonstrated in animal systems for R- and L-Type Ca^{2+} channels, such as Ca_v 1.3 (Bourinet et al., 1996; Rodriguez-Contreras et al., 2008; Rodriguez-Contreras and Yamoah, 2003). This scenario implies that Ca^{2+} channels in *S. apsteinii* have a different Sr fractionation behavior (i.e. relative permeability) than channels in other coccolithophores studied so far. Moreover, several other classes of Ca^{2+} transporters are capable of interacting with Sr^{2+}, such as Ca^{2+}-ATPases in corals (Allison et al., 2011), sodium/calcium exchangers (NCX) in archaea Liao et al., 2016), a mitochondrial calcium/proton exchanger (CAX; Tsai et al., 2014), and some TRP channels (Bouron et al., 2015). Therefore, intracellular Ca^{2+} transport in *S. apsteinii,* such as

CAX, NCX, and Ca^{2+}-ATPases, could, through higher Sr^{2+} permeability, potentially increase $[Sr^{2+}]$ at the site of calcification within CV.

A coccolithophore calcite fractionation model has recently been proposed in which the transport pathway of Ca^{2+} and Sr^{2+} is considered (Mejía et al., 2018). In this CaSri-Co model, the flux of Ca^{2+} and Sr^{2+} through plasma membrane transporters (F_{IN}) and the endoplasmic reticulum (F_{ER}) are used to calculate retention efficiency (F_{ER}/F_{IN}), which represents the pool of ions within the cell that can potentially be used for calcification. It follows that under circumstances in which transporter selectivity favors Sr^{2+} uptake, and retention efficiency is high, then coccolith Sr/Ca ratios can increase (Mejía et al., 2018). If *S. apsteinii* has a relatively high Sr^{2+} permeability through the Ca^{2+} transport pathway to the CV and a greater Ca^{2+} retention efficiency, then elevated CV $[Sr^{2+}]$ could occur. Additionally, the CaSri-Co model describes increased Sr/Ca corresponding to increased calcification rate (Mejía et al., 2018). Using published calcification rates (Gafar et al., 2019), we calculate that *S. apsteinii* exhibit over twice the calcification rate of *E. huxleyi* when normalized to cell surface area (0.45 pg/μm^2/d vs 0.18 pg/μm^2/d, respectively). Production of large, bulky *S. apsteinii* coccoliths therefore requires over twice the flux of Ca^{2+} per unit membrane surface area than *E. huxleyi*. A lower selectivity transport pathway under high ion flux scenarios has been proposed as a mechanism to explain patterns of Sr isotope and Sr/Ca fractionation in response to increased growth temperature in coccolithophores (Stevenson et al., 2014). While it is theoretically possible that a higher calcification rate alone could explain the increased CV Sr/Ca (relative to seawater) for *S. apsteinii*, it is likely that the higher Ca^{2+} flux rates combined with lower cation selectivity of Ca^{2+} transporters contribute to the remarkably high Sr/Ca relative to seawater in this species.

While atypical Ca^{2+} transporter selectivity is possible, it would have to be a specific feature of the Pontosphaeraceae (or even Scyphosphaera) because *Helicosphaera carteri* (also a member of the Zygodiscales) displays a fractionation against Sr (Sr/Ca of 3-4 mmol/mol), similar to the studied Coccolithales and Isochrysidales (Stoll et al., 2007b). As critical data on coccolithophore Ca^{2+} channels, pumps and exchangers is lacking, future work should assess the permeability of these transporters to Sr^{2+}.

There are, however, alternative explanations for the high D_{Sr} in *S. apsteinii*. Amorphous calcium carbonate (ACC) favors trace metal (Sr) incorporation into the crystal lattice structure in inorganic systems (Littlewood et al., 2017). Higher than expected Sr incorporation could theoretically be explained if *S. apsteinii* utilizes an ACC precursor phase for calcite precipitation. Although an ACC precursor is used in many biomineralization systems such as in foraminifera and mollusk shell formation (Addadi et al., 2006; De Nooijer et al., 2014), and has been considered as a possible intermediate in coccolithophore calcification (Brownlee et al., 2015), there is no current evidence for its use in coccolithophore biomineralization. While a 2016 study (Sviben et al.) described a Ca-P rich body in *E. huxleyi* that contained amorphous Ca phases, the authors conclude that it is not ACC. Instead these Ca-P rich bodies might act as an intermediary for Ca^{2+} transport (Sviben et al., 2016), which was confirmed by Gal et al., (2017) in series of pulse-chase experiments utilizing a Sr^{2+} tracer. Whether or not *S. apsteinii* utilizes such a compartment remains to be determined. Moreover, the hypothesis that *S. apsteinii* uses ACC while other coccolithophores do not implies species specific differences in calcification mechanisms at a basic level (mode of calcium carbonate precipitation).

Differences in calcification mechanisms at a higher level, such as species-specific coccolith associated polysaccharides (CAP; Fichtinger-Schepman et al., 1981; Marsh et al.,

2002), may influence Sr incorporation into calcite. CAP play an important role in coccolith morphogenesis, mainly as inhibitors of crystal growth (Borman et al., 1982; Marsh, 1994; Westbroek et al., 1984). A study using an inorganic system found that when using malonic acid to mimic the function of CAP by blocking acute calcite kink sites, D_{Sr} increased and *c*-axis elongation occurred as similarly seen in heterococcoliths (Payne et al., 2008). As this process mimics CAP-Sr interactions, it could explain the variable Sr incorporation seen among coccolithophore species. Additionally, the CaSri-Co model described by Mejía et al. (2018) acknowledges that organics can influence the Sr/Ca ratio, i.e. CAP, potentially using more CV Sr^{2+} for calcification. While species-specific CAP are likely playing the same functional role, their precise involvement in determining crystal growth and morphology could be subtly different among species. For example, some CAP influence crystal morphology by site-specific attachment to crystallographic steps (Henriksen et al., 2004), but others might not. *S. apsteinii* have CAP that are known to differ from those of some placolith bearing species, such as *C. braarudii* (Walker et al., 2018a). Relatively little is known about *S. apsteinii* CAP, but they are likely supplied by the closely associated reticular body that regulates fine scale coccolith morphology, and CAP are packed in between foliate crystals within coccoliths (Drescher et al., 2012).

We propose that differences in CAP structure or composition could explain variable Sr fractionation behavior in at least three ways: 1) intra coccolith vesicle CAP could alter the vesicle Ca^{2+} concentration needed to achieve super-saturation, which would in turn affect Sr fractionation (Langer et al., 2006). 2) Different CAP might have different Sr binding capacities or requirements, akin to brown algae polysaccharides (Davis et al. 2003), which might influence coccolith vesicle Sr/Ca. 3) Incorporation of CAP itself within coccoliths could introduce an

organic phase with an interspecific Sr/Ca. Because different kinds of CAP are used for different (partly morphogenetic) purposes (Marsh, 2000; Walker et al., 2018a), CAP-specific Sr fractionation offers a good explanation for inter as well as intra (see below) specific differences in Sr fractionation. Overall, we conclude that a combination of less selective Ca^{2+} transport and species-specific CAP likely influence Sr fractionation through several mechanisms.

4.2 Variable inter- and intra- coccolith Sr fractionation in S. apsteinii

The different Sr fractionation between muroliths and lopadoliths, and spatially within lopadoliths, was unexpected. Lopadolith bases and muroliths share morphological similarities, such as an outer lamellar ring, packed foliate crystals, and pores in the central region of the coccolith (Drescher et al., 2012). Lopadoliths arise through the extension of the lamellar ring and outer foliate crystals of a murolith to produce the wall of these structures. However, the base region of lopadoliths had higher D_{Sr} than muroliths. Because the structures share common crystal growth and orientation (Drescher et al. 2012), this cannot readily explain the observed disparity. The use of different CAP or an adjustment of the Ca^{2+} transport pathway associated with the production of lopadolith walls vs the murolith base could potentially underlie the varying Sr fractionation between these two coccolith types.

Secondary ion mass spectroscopy analysis of extant and microfossil placolith-bearing species such as *C. braarudii* and *Reticulofenestra bisecta* demonstrates spatially uniform minor element distribution (Grovenor et al., 2006; Prentice et al., 2014; Sucheras-Marx et al., 2016). This is in accordance with the prediction of a conceptual model (in its simplest form) describing Sr fractionation in *E. huxleyi* (Langer et al., 2006). While species-specific CAP-related Sr fractionation was discussed (Langer et al. 2006), a refined model should be developed to account for coccolith type-specific and intra coccolith Sr/Ca variability. However, the lopadolith gradient

should be interpreted with caution due to technical limitations of quantitative EDS when using unpolished specimens. Further work to resolve fine-scale distributions should be conducted using polished en-bloc samples combined with imaging mass spectrometry.

One advantage of the "CAP-hypothesis" is that it can potentially explain why D_{Sr} in *S. apsteinii* decreases with increasing seawater [Sr] (Table 3B): The resulting high coccolith vesicle Sr/Ca could possibly change CAP structure/conformation (Ishii et al., 1999; Kucerka et al., 2008) in such a way that the Ca^{2+} binding capacity of CAP increases (Woodward and Davidson, 1968). This increased Ca^{2+} binding capacity will then increase the vesicle [Ca^{2+}] concentration needed to achieve super-saturation with respect to calcite, which will in turn decrease D_{Sr} (Langer et al. 2006).

4.3 Sr is not required for morphogenesis in S. apsteinii

Because coccolith morphology was unaffected in *S. apsteinii* grown in a [Sr] that was over 25-fold lower than ambient (0.33 vs 9 mmol/mol), we conclude that Sr (i.e. elevated D_{Sr}) is not a requirement for coccolith morphogenesis of their unusually bulky coccoliths. On the contrary, higher [Sr] resulted in significant disruption of normal crystal morphogenesis as evidenced by a dramatic increase in the number of aberrant coccoliths produced. Although, we cannot rule out an inhibitory effect of elevated cellular [Sr] on the cell division machinery, like the cytoskeleton, which would also result in coccolith malformations (Langer et al., 2010). However, the lower growth rates for cultures grown in 72 mmol/mol Sr/Ca, and the inability of cells to grow in a media [Sr] above this, could be the result of a compromised coccosphere impeding their ability to properly divide. A similar effect was observed in *C. braarudii* in which calcification was disrupted using three separate approaches; Low Ca^{2+}, the metal chelator 1-hydroxyethane 1,1- diphosphonic acid (HEDP), and the Si analogue Ge (Walker et al., 2018b).

4.4 Why does high Sr/Ca disrupt S. apsteinii *coccolith morphogenesis?*

The increased frequency of Type R malformations in response to the 36 and 72 mmol/mol Sr/Ca treatments suggests the disruptive effect of high Sr on morphology is not purely through inorganic processes (Wasylenki et al., 2005). An inorganic mechanism of Sr-induced disruption would affect the whole coccolith, but Type R malformations are extremely site specific and leave most of the coccolith unaffected. As discussed above, CAP profoundly influence coccolith morphology (Borman et al., 1982). CAP bind divalent cations and their morphogenetic function depends on the ionic composition of the fluid (Davis et al., 2003; Grant et al., 1973; Henriksen and Stipp, 2009). Possibly, high CV Sr/Ca changes CAP structure/conformation (Ishii et al., 1999; Kucerka et al., 2008), which impairs their morphogenetic function (Henriksen and Stipp, 2009).

4.5 Concluding Remarks

S. apsteinii strongly fractionates for Sr resulting in coccolith Sr/Ca that is significantly higher than any other coccolithophore species (extant or extinct) for which this has been determined. Our results show that Sr is not necessary for normal murolith or lopadolith morphogenesis in this species. However, elevated levels of Sr in the medium disrupt coccolith morphogenesis and ultimately cell division, likely due to an incomplete coccosphere. We show that *S. apsteinii* fractionates Sr differently between and within coccolith types, suggesting Sr incorporation is not solely governed by a simple steady state Sr^{2+} and Ca^{2+} flux through the transport pathway to the CV. A variety of species-specific CAP that regulate morphogenesis may also contribute to the spatial and morphologically distinct Sr fractionation. Although Sr/Ca in coccoliths has been used to reconstruct past coccolithophore productivity, the coccolithophore Sr/Ca proxy remains poorly understood. Inter-and intraspecific organic phases could play a

critical role in minor element incorporation into coccoliths and therefore need to be considered when developing a mechanistic understanding of proxy relationships.

Acknowledgements

We thank Dr. Jack Pender at Eastern Carolina University for running seawater Sr analysis using ICP-MS. The work was supported by NSF GEO-NERC grant 1638838 to ART, European Research Council Grant ERC-ADG-670390 to CB and by Natural Environment Research Council grant NE/N011708/1. Analytical electron microscopy was performed in part at 1) Analytical Instrumentation Facility (AIF) at North Carolina State University, supported by the State of North Carolina and the National Science Foundation (award number ECCS-1542015) and 2) Joint School of Nanoscience and Nanoengineering, a member of the Southeastern Nanotechnology Infrastructure Corridor (SENIC) and National Nanotechnology Coordinated Infrastructure (NNCI), which is supported by the National Science Foundation (Grant ECCS-1542174).

Tables and Figures

Table 1: Published Sr/Ca (mmol/mol) and Sr partitioning coefficient (D_{Sr}) values for select coccolithophore species. Values included in this table reflect calcite Sr/Ca and D_{Sr} of cells under normal environmental conditions, that have not been potentially influenced by experimental manipulations. *values were calculated from published data assuming a seawater Sr/Ca of 9 mmol/mol.

Species	Sr/Ca (mmol/mol)	D_{Sr}	References
Emiliania huxleyi	~2.1 – 3.71	~0.1 – 0.5	Blanco-Ameijeiras et al., 2016 Langer et al., 2006 Müller et al., 2014 Müller et al., 2018 Rickaby et al., 2002 Stevenson et al., 2014
Gephyrocapsa oceanica	1.2 – 4.27	0.14 – 0.44	Hermoso et al., 2017 Müller et al., 2015 Stevenson et al., 2014
Coccolithus braarudii	2.4 – 3.9*	0.28 – 0.43	Müller et al., 2014 Müller et al., 2018 Stevenson et al., 2014
Calcidiscus quadriperforatus	2.67 – 3.10	0.32 – 0.37	Müller et al., 2014
Scyphosphaera apsteinii	22	2.5	Hermoso et al., 2017

Table 2. *S. apsteinii* murolith (A) and lapodolith (B) morphology in response to Sr. For each Sr treatment replicate, the morphology of between 62 – 85 muroliths and 37-61 lopadoliths were scored using an SEM (Refer to Fig. 2 for scoring categories). Values in the table are percentages, representing the average for 4 experimental replicates in which 40 cells were scored for morphology type and divided by the total muroliths or lopadoliths counted for that replicate. Type S: an incomplete lopadolith with normal calcite morphology. Type R: a lopadolith with longitudinal cleavage. Type T: an aberrant lopadolith with completely disorganized calcite.

A

Media [Sr] (µmol/L)	Media Sr/Ca (mmol/mol)	Normal Muroliths [± sd]	Incomplete Muroliths [± sd]	Malformed Muroliths [± sd]	Aberrant Muroliths [± sd]
3.4	0.33	**51.4** [7.8]	**21.3** [8.0]	**24.8** [3.8]	**2.5** [2.3]
90	9	**44.3** [6.8]	**20.3** [2.5]	**32.2** [3.2]	**3.3** [1.7]
360	36	**40.8** [4.2]	**23.5** [1.7]	**28.2** [3.2]	**7.5** [6.8]
720	72	**16.2** [2.3]	**29.0** [9.4]	**37.4** [5.3]	**17.4** [8.0]

B

Media [Sr] (µmol/L)	Media Sr/Ca (mmol/mol)	Normal Lopadoliths [± sd]	Malformed Lopadoliths [± sd]	Type S Lopadoliths [± sd]	Type R Lopadoliths [± sd]	Type T Lopadoliths [± sd]
3.4	0.33	**66.8** [12.7]	**11.6** [9.0]	**12.3** [3.3]	**7.0** [3.4]	**2.2** [2.6]
90	9	**46.9** [3.5]	**23.0** [4.7]	**22.5** [5.5]	**7.7** [7.3]	**0.0** [0.0]
360	36	**47.4** [12.3]	**20.8** [10.1]	**18.4** [9.4]	**11.4** [3.0]	**2.1** [4.2]
720	72	**14.5** [3.3]	**18.7** [7.1]	**20.0** [3.0]	**34.9** [10.4]	**11.9** [9.6]

Table 3 Sr incorporation and partitioning coefficients in *S. apsteinii* coccoliths. (A) The average calcite Sr/Ca mmol/mol ratio represents the amount of Sr relative to Ca in coccolith calcite (63 – 75 muroliths, 29 – 36 lopadolith bases, and 29-37 lopadolith tips), which significantly increases with increasing Sr media concentration ($p < 0.02$; t-test). **(B)** The average Sr partitioning coefficient (D_{Sr}), which exponentially decreases with increasing Sr media concentration ($p < 0.001$; t-test). For cells grown in the 0.33 mmol/mol Sr/Ca treatment Sr was below the technical LOD for EDS and not determined.

A

Media [Sr] (µmol/L)	Media Sr/Ca (mmol/mol)	Calcite Sr/Ca (all coccoliths) (mmol/mol) [± sd]	Murolith Sr/Ca (mmol/mol) [± sd]	Lopadolith Base Sr/Ca (mmol/mol) [± sd]	Lopadolith Tip Sr/Ca (mmol/mol) [± sd]
3.4	0.33	ND	ND	ND	ND
90	9	**27.0** [10.8]	**22.9** [10.6]	**33.6** [8.51]	**28.8** [9.87]
360	36	**36.8** [18.3]	**31.7** [16.7]	**45.4** [16.3]	**40.7** [19.2]
720	72	**51.3** [27.1]	**39.6** [23.4]	**62.9** [24.8]	**59.9** [23.3]

B

Media [Sr] (µmol/L)	Media Sr/Ca (mmol/mol)	Total Average D_{Sr} [± sd]	Murolith D_{Sr} [± sd]	Lopadolith Base D_{Sr} [± sd]	Lopadolith Tip D_{Sr} [± sd]
3.4	0.33	ND	ND	ND	ND
90	9	**3.00** [1.20]	**2.54** [1.18]	**3.74** [0.95]	**3.20** [1.10]
360	36	**1.02** [0.51]	**0.88** [0.46]	**1.26** [0.45]	**1.13** [0.53]
720	72	**0.71** [0.38]	**0.55** [0.33]	**0.87** [0.34]	**0.83** [0.32]

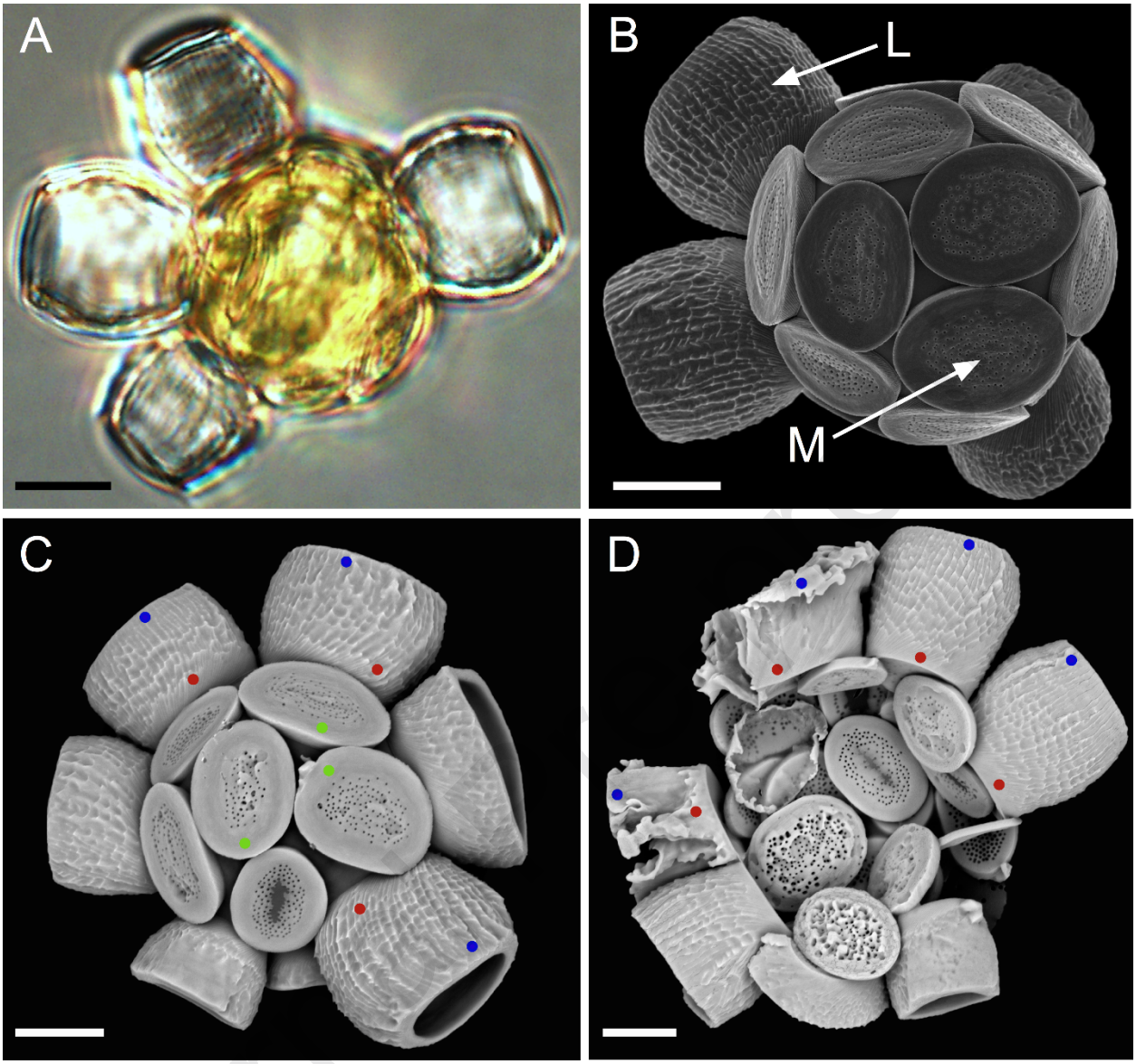

Figure 1: ***Scyphosphaera apsteinii*** **morphology**

A light (A) and SEM (B) micrograph of *S. apsteinii* displaying dimorphic morphology. M = muroliths. L = lopadoliths. C, D are SEM micrographs of *S. apsteinii* grown in 9 and 72 mmol/mol Sr/Ca, respectively, with region-of-interest (ROI) (circles) demonstrating how spectra were collected from muroliths (green) and lopadolith bases (red) and tips (blue). Scale bars represent 5 µm.

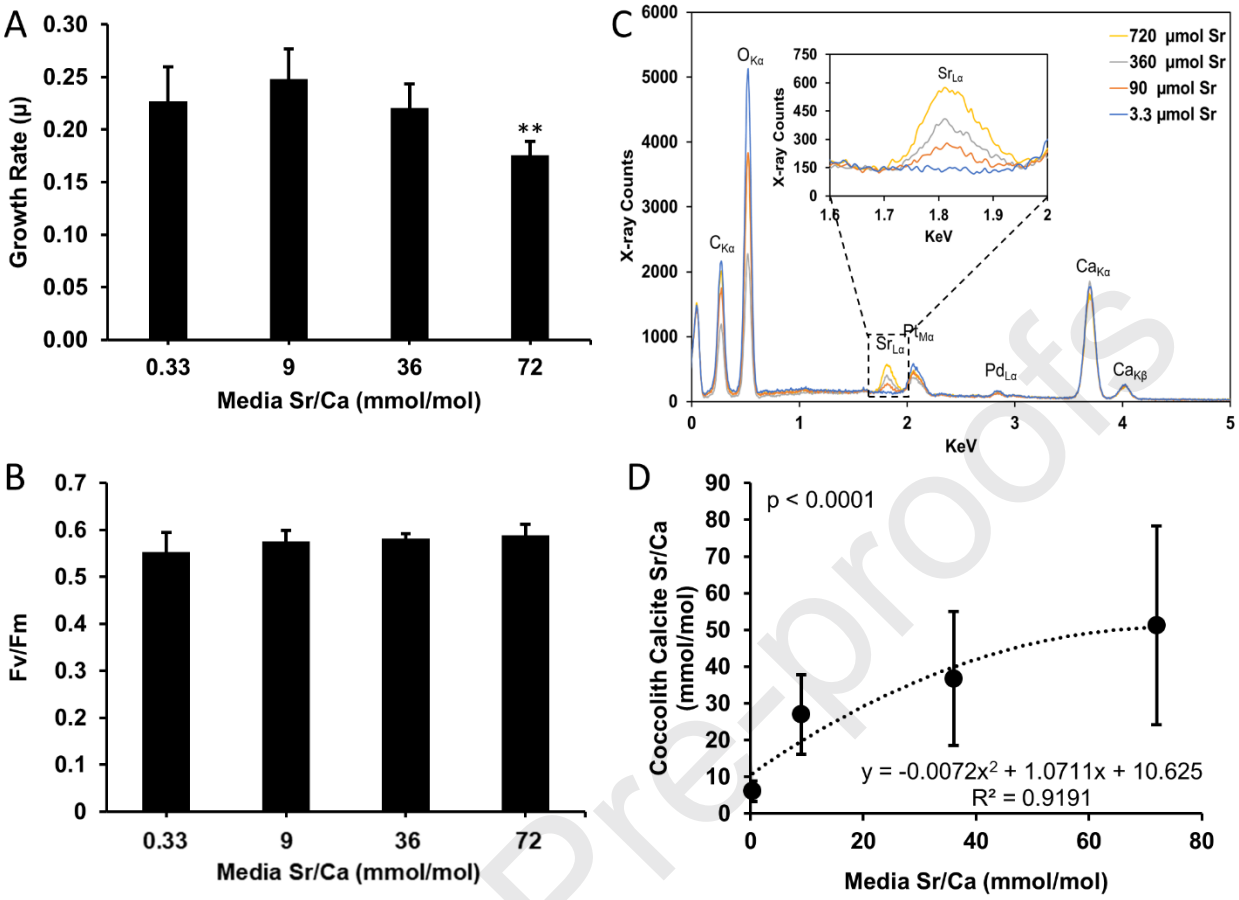

Figure 2. Growth and physiology of *S. apsteinii* in response to Sr enrichment

(A) Maximum growth rate (μ) of *S. apsteinii* determined over 10 d in deplete, ambient, or enriched Sr treatments (N = 4 independent replicates for each Sr treatment ± SD). **(B)** Quantum yield of photosystem II (F_v/F_m) of dark-adapted *S. apsteinii* cells grown under the same Sr/Ca (N = 4 independent replicates for all Sr treatments ± SD). **(C)** Example EDS spectra showing increased Sr incorporation for *S. apsteinii* coccoliths grown in deplete, ambient, and enriched Sr. Insert: detail of the EDS spectra showing Sr peaks among Sr treatments. **(D)** Average Sr/Ca (± SD) of *S. apsteinii* calcite increases with media Sr/Ca mmol/mol. Lopadoliths and muroliths were combined resulting in 64-77 coccoliths for each treatment. The data were fit with a polynomial relationship ($r^2 = 0.92$) and significant differences were determined between all Sr treatments ($p < 0.001$, ANOVA with Dunn's Pairwise Comparison).

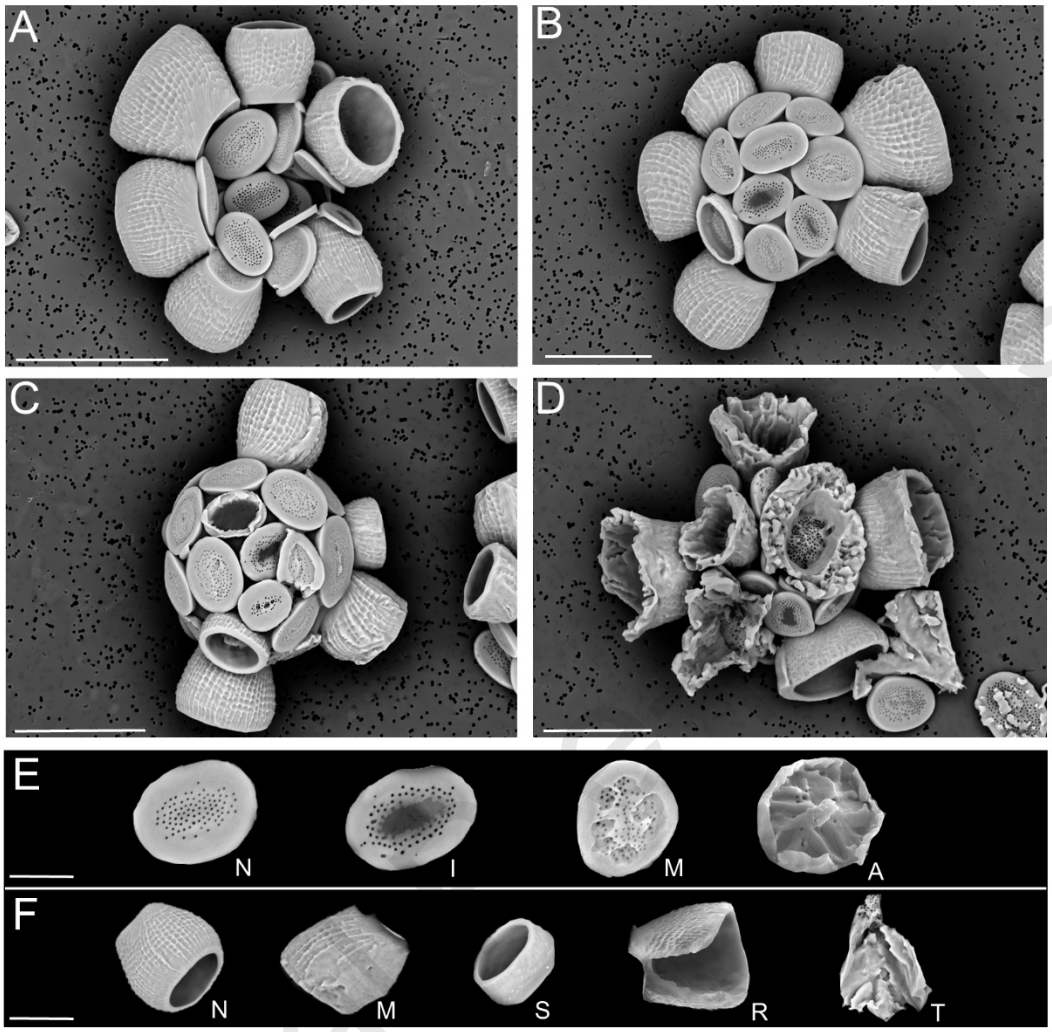

Figure 3. Effect of Sr on *S. apsteinii* coccolith morphology

SEM images acquired with an electron backscatter detector showing the effects of **(A**) deplete, **(B)** ambient, and **(C, D)** high (36 mmol/mol Sr/Ca and 72 mmol/mol Sr/Ca, respectively) Sr on *S. apsteinii* coccolith morphology. Scale bars represent 20 μm. **(E)** Examples of murolith morphology scoring categories from left to right: normal, incomplete, malformed, and aberrant. Scale bar represents 5 μm. **(F)** Examples of lopadolith morphology scoring categories from left to right: normal, malformed (minor malfunctions commonly seen in control cultures), Type S (a short lopadolith with normal morphology), Type R (longitudinal cleavage or sharp edging of lopadolith tip), and Type T (aberrant, completely disorganized calcite).

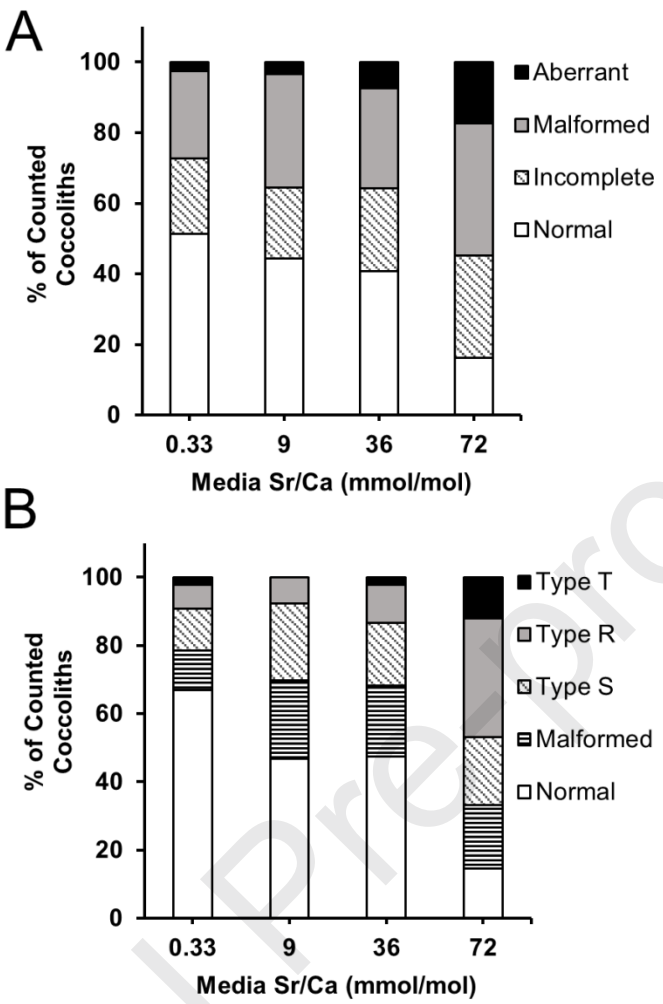

Figure 4. Increased Sr causes an increase in malformed and aberrant coccoliths produced by *S. apsteinii*

(A) Percentage of normal, incomplete, malformed, and aberrant *S. apsteinii* muroliths in coccospheres of cells grown in deplete, ambient, and high Sr (± SD). Percentages represent the average for 4 experimental replicates in which 62-85 muroliths from 40 cells were scored for morphology type and divided by the total muroliths counted for that replicate. **(B)** Percentage of normal, malformed, Type S, Type R, and Type T *S. apsteinii* lopadoliths (see Fig. 2) from cells grown in deplete, ambient, and high Sr (37-61 lopadoliths from 40 cells from 4 replicate cultures were scored for each Sr treatment ± SD). See Table 2 for details.

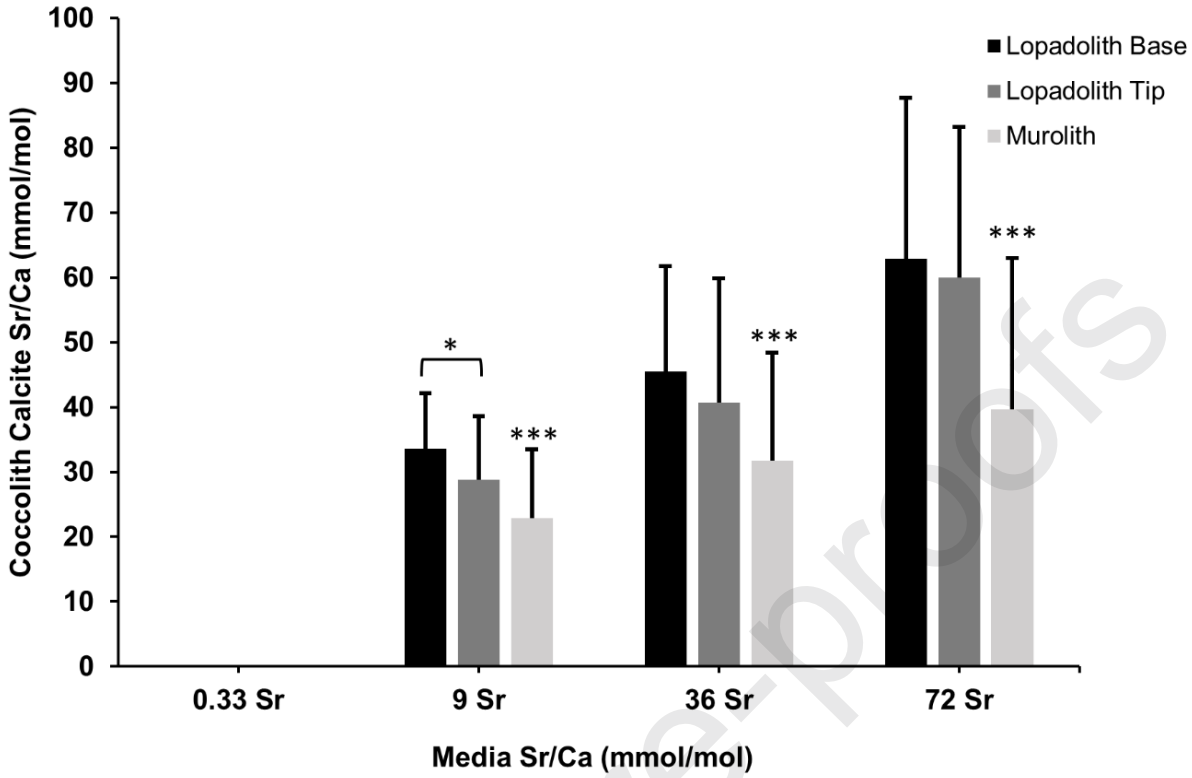

Figure 5. Average Sr/Ca mmol/mol in *S. apsteinii* coccoliths by morphotype in response to increasing media [Sr]

Average calcite Sr/Ca mmol/mol values (± SD, $N_{muroliths}$ = 63-75; $N_{lopadolith\ base}$ = 29-36; $N_{lopadolith\ tip}$ = 29-37 coccoliths from each experimental treatment) were calculated using Eq. 1 for muroliths and lopadoliths. The EDS limit of detection (LOD) for Sr was calculated to be 2.29 mmol/mol Sr/Ca. Calculated calcite Sr/Ca values for cells from the 0.33 Sr/Ca mmol/mol treatment were technically at or below LOD for the EDS method and were not further analyzed. See Table 3 for details.

5.0 Research Data

Research Data associated with this article can be accessed at https://doi.org/10.17632/3swtykz23k.1

6.0 Citations

Addadi, L., Joester, D., Nudelman, F. and Weiner, S. (2006) Mollusk shell formation: A source of new concepts for understanding biomineralization processes. *Chem.: Eur. J.* **12,** 981-987.

Aimaiti, A., Maimaitiyiming, A., Boyong, X., Aji, K., Li, C., and Cui, L. (2017) Low-dose strontium stimulates osteogenesis but high-dose doses cause apoptosis in human adipose-derived stem cells via regulation of the ERK1/2 signaling pathway. *Stem Cell Res. Ther.* **8**, 1-12.

Allison, N., Cohen, I., Finch, A.A., Erez, J., and EMIF. (2011) Controls on Sr/Ca and Mg/Ca in scleractinian corals: The effects of Ca-ATPase and transcellular Ca channels on skeletal chemistry. *Geochim. Cosmochim. Ac.* **75**, 6350-6360.

Balch, W. M. (2018) The Ecology, Biogeochemistry, and Optical Properties of Coccolithophores. *Annu. Rev. Mar. Sci.* **10,** 71-98.

Blanco-Ameijeiras, S., Lebrato, M., Stoll, H.M., Iglesias-Rodriguez, D., Müller, M.N., Méndez-Vicente, A., and Oschlies, A. (2016) Phenotypic variability in the coccolithophore *Emiliania huxleyi*. *Plos One* **11: e0157697,** 1-17.

Borman, A. H., Dejong, E. W., Huizinga, M., Kok, D. J., Westbroek, P. and Bosch, L. (1982) The role in $CaCO_3$ crystallization of an acid Ca^{2+} binding polysaccharide associated with coccoliths of *Emiliania-huxleyi*. *Eur. J. Biochem.* **129,** 179-183.

Bourinet, E., Zamponi, G. W., Stea, A., Soong, T. W., Lewis, B. A., Jones, L. P., Yue, D. T. and Snutch, T. P. (1996) The alpha(1E) calcium channel exhibits permeation properties similar to low-voltage-activated calcium channels. *J. Neurosci.* **16,** 4983-4993.

Bouron, A., Kiselyov, K., and Oberwinkler, J. (2015) Permeation, regulation and control of expression of TRP channels by trace metal ions. *Eur. J. Physiol.* **467**, 1143-1164.

Brownlee, C. and Taylor, A. (2004) Calcification in coccolithophores: A cellular perspective. In: *Coccolithophores: from Molecular Processes to Global Impact* (eds H.R. Thierstein and J.R. Young). Springer, Berlin. pp. 31-49.

Brownlee, C., Wheeler, G. L. and Taylor, A. R. (2015) Coccolithophore biomineralization: New questions, new answers. *Semin. Cell Dev. Biol.* **46,** 11-16.

Daniels, C. J., Poulton, A. J., Balch, W. M., Maranon, E., Adey, T., Bowler, B. C., Cermeno, P., Charalampopoulou, A., Crawford, D. W., Drapeau, D., Feng, Y. Y., Fernandez, A., Fernandez, E., Fragoso, G. M., Gonzalez, N., Graziano, L. M., Heslop, R., Holligan, P. M., Hopkins, J., Huete-Ortega, M., Hutchins, D. A., Lam, P. J., Lipsen, M. S., Lopez-Sandoval, D. C., Loucaides, S., Marchetti, A., Mayers, K. M. J., Rees, A. P., Sobrino, C., Tynan, E. and Tyrre, T. (2018) A global compilation of coccolithophore calcification rates. *Earth Syst. Sci. Data* **10,** 1859-1876.

Davis, T. A., Volesky, B. and Mucchi, A. (2003) A review of the biochemistry of heavy metal biosorption by brown algae. *Water Res.* **37,** 4311-4330.

De Nooijer, L. J., Spero, H. J., Erez, J., Bijma, J. and Reichart, G. J. (2014) Biomineralization in perforate foraminifera. *Earth-Sci. Rev.* **135,** 48-58.

De Villiers, S. (1999) Seawater strontium and Sr/Ca variability in the Atlantic and Pacific oceans. *Earth Planet. Sc. Lett.* **171,** 623-634.

Drescher, B., Dillaman, R. M. and Taylor, A. R. (2012) Coccolithogenesis in *Scyphosphaera apsteinii* (Prymnesiophyceae). *J. Phycol.* **48,** 1343-1361.

Fichtinger-Schepman, A. M., Kamerling, J. P., Versluis, C. and Vliegenthart, J. F. G. (1981) Structural studies of the methylated, acidic polysaccharide associated with coccoliths of *Emiliania-huxleyi* (Lohmann) Kamptner. *Carbohydr. Res.* **93,** 105-123.

Flores, J. A., Sierro, F. J., Frances, G., Vazquez, A. and Zamarreno, I. (1997) The last 100,000 years in the western Mediterranean: Sea surface water and frontal dynamics as revealed by coccolithophores. *Mar. Micropaleontol.* **29,** 351-366.

Fowler, N., Tomas, C., Baden, D., Campbell, L. and Bourdelais, A. (2015) Chemical analysis of *Karenia papilionacea*. *Toxicon.* **101,** 85-91.

Gafar, N. A., Eyre, B. D. and Kai, G. S. (2019) A comparison of species specific sensitivities to changing light and carbonate chemistry in calcifying marine phytoplankton. *Sci. Rep.* **9:2486,** 1-12.

Gal, A., Sviben, S., Wirth, R., Schreiber, A., Lassalle-Kaiser, B., Faivre, D. and Scheffel, A. (2017) Trace-element incorporation into intracellular pools uncovers calcium-pathways in a coccolithophore. *Adv. Sci.* **4,** 5.

Grant, G. T., Morris, E. R., Rees, D. A., Smith, P. J. C. and Thom, D. (1973) Biological interactions between polysaccharides and divalent cations - egg-box model. *FEBS Lett.* **32,** 195-198.

Grovenor, C. R. M., Smart, K. E., Kilburn, M. R., Shore, B., Dilworth, J. R., Martin, B., Hawes, C. and Rickaby, R. E. M. (2006) Specimen preparation for NanoSIMS analysis of biological materials. *Appl. Surf. Sci.* **252,** 6917-6924.

Henriksen, K. and Stipp, S. L. S. (2009) Controlling biomineralization: The effect of solution composition on coccolith polysaccharide functionality. *Cryst. Growth Des.* **9,** 2088-2097.

Henriksen, K., Stipp, S. L. S., Young, J. R. and Marsh, M. E. (2004) Biological control on calcite crystallization: AFM investigation of coccolith polysaccharide function. *Am. Min.* **89,** 1709-1716.

Hermoso, M. (2014) Coccolith-derived isotopic proxies in palaeoceanography: where geologists need biologists. *Cryptogamie Algol.* **35,** 323-351.

Hermoso, M., Lefeuvre, B., Minoletti, F. and De Rafelis, M. (2017) Extreme strontium concentrations reveal specific biomineralization pathways in certain coccolithophores with implications for the Sr/Ca paleoproductivity proxy. *Plos One* **12: e018565,** 1-16.

Hopkins, J. and Balch, W. M. (2018) A new approach to estimating coccolithophore calcification rates from space. *J. Geophys. Res.-Biogeo.* **123,** 1447-1459.Ishii, T., Matsunaga, T., Pellerin, P., O'neill, M. A., Darvill, A. and Albersheim, P. (1999) The plant cell wall polysaccharide rhamnogalacturonan II self-assembles into a covalently cross-linked dimer. *J. Biol. Chem.* **274,** 13098-13104.

Kester, D. R., Duedall, I. W., Connors, D. N. and Pytkowicz, R. M. (1967) Preparation of artificial seawater. *Limnol. Oceanogr.* **12,** 176-179.

Kozhevnikova, A.D., Seregin, I.V., Bystrova, E.I., Belyaeva, A.I., Kataeva, M.N., and Ivanov, V.B. (2009) The effects of lead, nickel, and strontium nitrates on cell division and elongation in maize roots. *Russ. J. Plant Physiol.* **56**, 242-250.

Krumhardt, K. M., Lovenduski, N. S., Iglesias-Rodriguez, M. D. and Kleypas, J. A. (2017) Coccolithophore growth and calcification in a changing ocean. *Prog. Oceanogr.* **159,** 276-295.

Kucerka, N., Papp-Szabo, E., Nieh, M. P., Harroun, T. A., Schooling, S. R., Pencer, J., Nicholson, E. A., Beveridge, T. J. and Katsaras, J. (2008) Effect of cations on the structure of bilayers formed by lipopolysaccharides isolated from *Pseudomonas aeruginosa* PAO1. *J. Phys. Chem. B* **112,** 8057-8062.

Langer, G., De Nooijer, L. J. and Oetjen, K. (2010) On the role of the cytoskeleton in coccolith morphogenesis: The effect of cytoskeleton inhibitors. *J. Phycol.* **46,** 1252-1256.

Langer, G., Gussone, N., Nehrke, G., Riebesell, U., Eisenhauer, A., Kuhnert, H., Rost, B., Trimborn, S. and Thoms, S. (2006) Coccolith strontium to calcium ratios in *Emiliania huxleyi*: The dependence on seawater strontium and calcium concentrations. *Limnol. Oceanogr.* **51,** 310-320.

Liao, J., Marinelli, F., Lee, C., Huang, Y., Feraldo-Gomez, J.D., and Jiang, Y. (2016) Mechanism of extracellular ion exchange and binding-site occlusion in the sodium-calcium exchanger. *Nat. Struct. Mol. Biol.* **23**, 590-599.

Littlewood, J. L., Shaw, S., Peacock, C. L., Bots, P., Trivedi, D. and Burke, I. T. (2017) Mechanism of enhanced strontium uptake into calcite via an amorphous calcium carbonate crystallization pathway. *Cryst. Growth Des.* **17,** 1214-1223.

Mackinder, L., Wheeler, G., Schroeder, D., Riebesell, U. and Brownlee, C. (2010) Molecular mechanisms underlying calcification in coccolithophores. *Geomicrobiol. J.* **27,** 585-595.

Marsh, M. E. (1994) Polyanion-mediated mineralization - assembly and reorganization of acidic polysaccharides in the golgi system of a coccolithophorid alga during mineral deposition. *Protoplasma* **177,** 108-122.

Marsh, M. E. (2000) Polyanions in the $CaCO_3$ mineralization of coccolithophores. In: *Biomineralization: from biology to biotechnology and medical application.* (ed E. Bauerlein). Wiley-VCH, Weinheim. pp. 251-268.

Marsh, M. E. (2003) Regulation of $CaCO_3$ formation in coccolithophores. *Comp. Biochem. Phys. B* **136,** 743-754.

Marsh, M. E., Ridall, A. L., Azadi, P. and Duke, P. J. (2002) Galacturonomannan and Golgi-derived membrane linked to growth and shaping of biogenic calcite. *J. Struct. Biol.* **139,** 39-45.

Mejía. L.M., Paytan, A., Eisenhauer, A., Böhm, F., Kolevica, A., Bolton, C., Méndez-Vicente, A., Abrevaya, L., Isensee, K., and Stoll, H. (2018) Controls over $\delta^{44/40}$Ca and Sr/Ca variations in coccoliths: New perspectives from laboratory cultures and cellular models. *Earth Planet. Sc. Lett.* **481,** 48-60.

Milliman, J. D. (1993) Production and Accumulation of Calcium-Carbonate in the Ocean - Budget of a Nonsteady State. *Global Biogeochem. Cy.* **7,** 927-957.

Müller, M.N., Lebrato, M., Riebesell, U., Barcelos e Ramos, J., Schulz, K.G., Blanco-Ameijeiras, S., Sett, S., Eisenhauer, A., and Stoll., H.M. (2014) Influence of temperature and CO_2 on the strontium and magnesium composition of coccolithophore calcite. *Biogeosciences* **11**, 1065 – 1075.

Müller, M. N., Krabbenhoft, A., Vollstaedt, H., Brandini, F. P. and Eisenhauer, A. (2018) Stable isotope fractionation of strontium in coccolithophore calcite: Influence of temperature and carbonate chemistry. *Geobiology* **16,** 297-306.

Outka, D. E. and Williams, D. C. (1971) Sequential Coccolith Morphogenesis in *Hymenomonas carterae*. *J. Protozool.* **18,** 285-297.

Payne, V. E., Rickaby, R. E. M., Benning, L. G. and Shaw, S. (2008) Calcite crystal growth orientation: implications for trace metal uptake into coccoliths. *Mineral. Mag.* **72,** 269-272.

Prentice, K., Dunkley Jones, T., Lees, J., Young, J., Bown, P., Langer, G., Fearn, S. and Eimf (2014) Trace metal (Mg/Ca and Sr/Ca) analyses of single coccoliths by Secondary Ion Mass Spectrometry. *Geochim. Cosmochim. Ac.* **146,** 90-106.

Rickaby, R. E. M., Schrag, D. P., Zondervan, I. and Riebesell, U. (2002) Growth rate dependence of Sr incorporation during calcification of *Emiliania huxleyi*. *Global Biogeochem. Cy.* **16,** 8.

Rodriguez-Contreras, A., Lv, P., Zhu, J., Kim, H. J. and Yamoah, E. N. (2008) Effects of strontium on the permeation and gating phenotype of calcium channels in hair cells. *J. Neurophysiol.* **100,** 2115-2124.

Rodriguez-Contreras, A. and Yamoah, E. N. (2003) Effects of permeant ion concentrations on the gating of L-type Ca2+ channels in hair cells. *Biophys. J.* **84,** 3457-3469.

Saavedra-Pellitero, M., Baumann, K. H., Ullermann, J. and Lamy, F. (2017) Marine Isotope Stage 11 in the Pacific sector of the Southern Ocean; a coccolithophore perspective. *Quat. Sci. Rev.* **158,** 1-14.

Stevenson, E. I., Hermoso, M., Rickaby, R. E. M., Tyler, J. J., Minoletti, F., Parkinson, I. J., Mokadem, F. and Burton, K. W. (2014) Controls on stable strontium isotope fractionation in coccolithophores with implications for the marine Sr cycle. *Geochim. Cosmochim. Ac.* **128,** 225-235.

Stoll, H. M., Rosenthal, Y. and Falkowski, P. (2002a) Climate proxies from Sr/Ca of coccolith calcite: Calibrations from continuous culture of Emiliania huxleyi. *Geochim. Cosmochim. Ac.* **66,** 927-936.

Stoll, H. M. and Schrag, D. P. (2000) Coccolith Sr/Ca as a new indicator of coccolithophorid calcification and growth rate. *Geochem. Geophys. Geosyst.* **1,** 24.

Stoll, H. M., Shimizu, N., Archer, D. and Ziveri, P. (2007a) Coccolithophore productivity response to greenhouse event of the Paleocene-Eocene Thermal Maximum. *Earth Planet. Sc. Lett.* **258,** 192-206.

Stoll, H. M., Ziveri, P., Geisen, M., Probert, I. and Young, J. R. (2002b) Potential and limitations of Sr/Ca ratios in coccolith carbonate: new perspectives from cultures and monospecific samples from sediments. *Philos. T. R. Soc. A* **360,** 719-747.

Stoll, H. M., Ziveri, P., Shimizu, N., Conte, M. and Theroux, S. (2007b) Relationship between coccolith Sr/Ca ratios and coccolithophore production and export in the Arabian Sea and Sargasso Sea. *Deep-Sea Res. Pt. II* **54,** 581-600.

Sucheras-Marx, B., Giraud, F., Simionovici, A., Daniel, I. and Tucoulou, R. (2016) Perspectives on heterococcolith geochemical proxies based on high-resolution X-ray fluorescence mapping. *Geobiology* **14,** 390-403.

Sun, S. Y., Liu, M. X., Nie, X. Q., Dong, F. Q., Hu, W. Y., Tan, D. Y. and Huo, T. T. (2018) A synergetic biomineralization strategy for immobilizing strontium during calcification of the coccolithophore *Emiliania huxleyi*. *Environ. Sci. Pollut. R.* **25,** 22446-22454.

Sviben, S., Gal, A., Hood, M.A., Bertinetti, L., Politi, Y., Bennet, M., Krishnamoorthy, P., Schertel, A., Wirth, R., Sorrentino, A., Pereiro, E., Faivre, D., and Scheffel, A. (2016) A vacuole-like compartment concetrates a disorded caclium phase in a key coccolithophorid alga. *Nat. Commun.* **7:11228**, 1 – 9.

Taylor, A. R., Brownlee, C., Wheeler, G. and Annual, R. (2017) Coccolithophore Cell Biology: Chalking Up Progress. *Annu. Rev. Mar. Sci.* **9**, 283-310.

Tsai, M., Jiang, D., Zhao, L., Clapham, D., and Miller, C. (2014) Functional reconstruction of the mitochondrial Ca^{2+}/H^{+} antiporter Letm1. *J. Gen. Physiol.* **143**, 67-73.

Walker, C. E., Heath, S., Salmon, D. L., Smirnoff, N., Langer, G., Taylor, A. R., Brownlee, C. and Wheeler, G. L. (2018a) An Extracellular Polysaccharide-Rich Organic Layer Contributes to Organization of the Coccosphere in Coccolithophores. *Front. Mar. Sci.* **5,** 12.

Walker, C. E., Taylor, A. R., Langer, G., Durak, G. M., Heath, S., Probert, I., Tyrrell, T., Brownlee, C. and Wheeler, G. L. (2018b) The requirement for calcification differs between ecologically important coccolithophore species. *New Phytol.* **220,** 147-162.

Wasylenki, L. E., Dove, P. M., Wilson, D. S. and De Yoreo, J. J. (2005) Nanoscale effects of strontium on calcite growth: An in situ AFM study in the absence of vital effects. *Geochim. Cosmochim. Ac.* **69,** 3017-3027.

Westbroek, P., Dejong, E. W., Vanderwal, P., Borman, A. H., Devrind, J. P. M., Kok, D., Debruijn, W. C. and Parker, S. B. (1984) Mechanism of calcification in the marine alga *Emiliania-huxleyi*. *Philos. Trans. R. Soc. Lond. B Biol. Sci.* **304,** 435-&.

Woodward, C. and Davidson, E. A. (1968) Structure-function relationships of protein polysaccharide complexes - specific ion-binding properties. *Proc. Natl. Acad. Sci. U.S.A.* **60,** 201-205.

Young, J. R., Davis, S. A., Bown, P. R. and Mann, S. (1999) Coccolith ultrastructure and biomineralisation. *J. Struct. Biol.* **126,** 195-215.

Young, J. R., Poulton, A. J. and Tyrrell, T. (2014) Morphology of *Emiliania huxleyi* coccoliths on the northwestern European shelf - is there an influence of carbonate chemistry? *Biogeosciences* **11,** 4771-4782.

Declaration of interests

☒ The authors declare that they have no known competing financial interests or personal relationships that could have appeared to influence the work reported in this paper.

☐The authors declare the following financial interests/personal relationships which may be considered as potential competing interests: